Rev.Adv.Mater.Sci. 22(2009) 1-20

SYNTHESIS, STRUCTURE AND PROPERTIES OF NANOSIZED SILICON CARBIDE

R.A. Andrievski

Institute of Problems of Chemical Physics, Russian Academy of Sciences, Semenov prospect, 1, Chernogolovka, Moscow Region 142432, Russia

Received: November 05, 2009

Abstract. Features of synthesis of particles, wires, tubes, films and bulk materials based on silicon carbide in nanocrystalline/amorphous condition are considered. The main attention is taken to the preparation of nanotubes/nanowires, films and nanosized SiC inclusions in matrixes. Their structure, physical, chemical and mechanical properties are discussed in connection with the influence of size effects and other features in detail. Such new results, as the hardness essential increase, display of the nanowire high plasticity, substantial in crease of photoluminescence spectra intensity, biocompatibility, good resistance to amorphization under irradiation and so on, are described. Applications in electronics, optics, nanotechnics and medicine are pointed. Some unresolved problems are underlined.

1. INTRODUCTION

Thanks to a wide spectrum of physical, chemical and mechanical properties and according to extensive application, the mono - and polycrystal materials based on silicon carbide draw for a long time a great attention (see, for example, only the last proceedings [1-3] reflecting works of the largest International conferences in 2006-2008). Some data about nanocrystalline SiC (as of 2005) have been reflected in the present author reviews [4,5] devoted to all range of high-melting point compounds. However, the number of publications on this topic as well as the general information stream in the nanotechnology area [6] more and more extends. According to SCOPUS base, in 2008 about 150 articles has been devoted to nanocrystalline and amorphous objects on the SiC base. In addition to indicators known earlier such as high strength, corrosion stability and perspective semiconductor properties, the interesting biological, sensor and optical characteristics of silicon carbide are revealed. It has generated a need for the analysis of last tendencies in researches and developments devoted to nanomaterials-based SiC. Unlike to data [4,5], the attention will be concentrated and on amorphous nanosubjects as for silicon carbide considerable propensity to amorphization is characteristic.

As it is known, silicon carbide crystallizes in many polytypes of so-called polymorphs in one measurement (their total amount is more than 200 [7]). For convenience of the further statement and comparison with nanosubjects, some characteristics of the most widespread polytypes are shown in Table 1 [7-9] and positions in the carbon and silicon atoms arrangement and structures are demonstrated in Fig. 1. The SiC polytype content is defined by conditions of preparation (temperature, pressure and environment) and presence of impurities. It is considered that cubic polytype 3C-SiC is more stable in comparison with other hexagonal polytypes up to temperature of ~2100 °C [8].

Corresponding author: R.A. Andrievski, e-mail: ara@icp.ac.ru

Table 1. The main physical/chemical properties of the most widespread SiC polytypes [7-9].

Property	POLYTYPE			
	3C-SiC (β–SiC)	2H-SiC (α–SiC)	4H-SiC (α–SiC)	6H-SiC (α–SiC)
Space group	*F*43*m*	$P6_3mc$	$P6_3mc$	$P6_3mc$
Hexagonality (%)	0	100	50	33
Stacking order (See Fig. 1)	ABC	AB	ABCB	ABCACB
Lattice constant *a* (nm)	0.43589-0.43596	0.30753-0.3081	0.3070-0.3081	0.3073-0.3081
Lattice constant *c* (nm)	–	0.5031-0.5048	1.0053-1.008	1.51092-1.512
Density (g/cm^3)	3.215	3.219	3.215	3.212
Band gap (eV)	2.39	3.33	3.26	3.0
Thermal conductivity (W cm^{-1} K^{-1})	3.6	–	4.9	4.9
Electron mobility (cm^2 V^{-1}s^{-1}, 300K)	≤1000	–	≤850	≤450
Hole mobility (cm^2 V^{-1}s^{-1}, 300K)	≤40	–	≤120	≤100
Electrical resistivity (Ω cm)	$10^2 – 10^3$			

2. FEATURES OF SYNTHESIS

2.1. Nanopowders, nanoparticles in matrices, nanoporous structures, nanowires and nanotubes

Nanosized silicon carbide powders are manufactured for a long time already by several companies. For example, PlasmaChem GmbH (Germany) delivers the SiC nanopowder with the average size of particles 20±7 nm and purity> 95% (free silicon <0.75%; oxygen <1.25%; chlorine <0.25%). Among new works on the SiC nanopowder synthesis it seems to be interesting to mark out the following most interesting investigations:

- synthesis of amorphous SiC nanoparticles using the low pressure microwave plasma [10],
- controlled synthesis of β-SiC nanopowders using inductively coupled plasma [11],
- synthesis α-SiC nanocrystals by carbothermic reduction [12].

The as-prepared amorphous SiC particles were synthesized from the decomposition of tetramethylsilane precursor in a plasma operated at room temperature and low precursor partial pressure (0.001-0.02 Torr) using argon as carrier gas (3 Torr) [10]. The synthesis conditions were varied to prepare nanoparticles in the size 4-6 nm with reasonable monodispersity confirmed by transmission electron microscopy (TEM) characterization. The high organic content and excess carbon presented in the as-synthesized powder particles were fixed by X-ray photoelectron spectroscopy (XPS) and Fourier-Transformed Infrared (FTIR) spectroscopy. Additional annealing the samples in argon at 800 °C for 30 min results in transformation of the amorphous SiC to crystalline β-SiC and graphite. Further studies for commercial scale production of SiC nanoparticles smaller than 10 nm are continuing.

Other proposition in obtaining large amount of SiC nanopowder consist in introducing coarse SiC powders (with an average size about 1-3 μm) inside the dense plasma formed by the inductively coupled plasma torch [11]. The evaporation/condensation process study results in preparation of β-SiC cubic phase nanoparticles with variable stoichiometry and mean size of around 30 nm. Further investigations are now in progress in order to obtain a pure β-SiC and to control the particle size together with size distribution.

Carbothermic synthesis of spherical amorphous SiO_2 nanoparticles (size of 2-10 nm) with sucrose at 1500 °C (with additional annealing at 700 °C for decarburization) results in preparation of powders with typical size of 5-10 nm [12]. The X-ray diffraction (XRD) study revealed the availability 6H- and

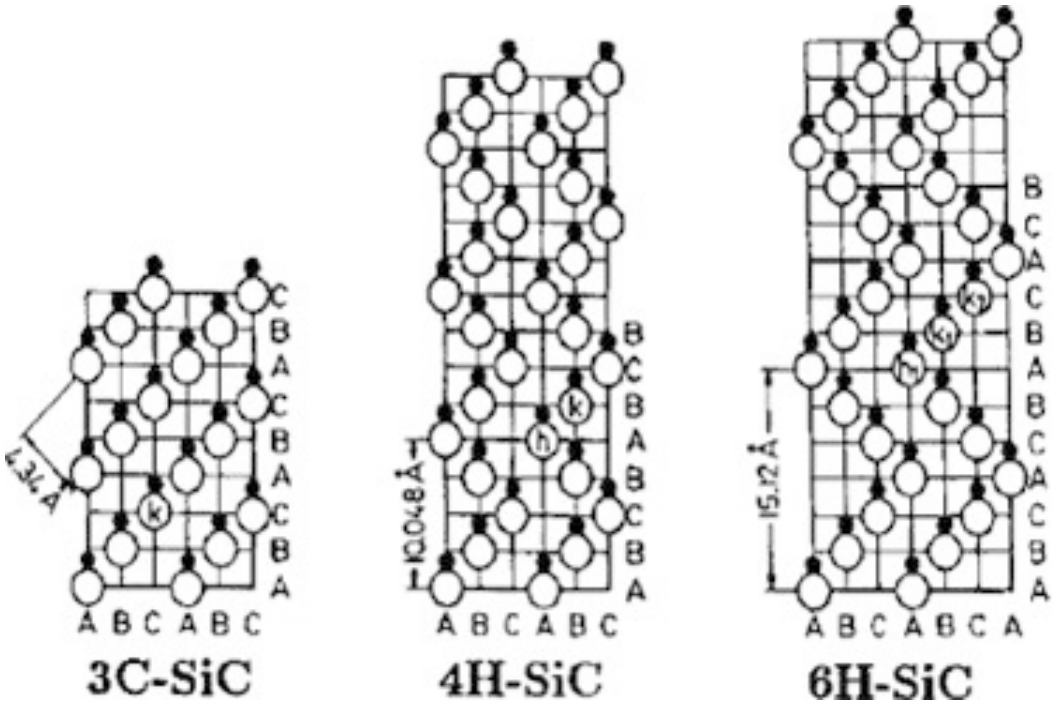

Fig. 1. Positions of carbon (●) and silicon (O) atoms in the (112-0) plane for various SiC polytypes [7]. Reprinted with permission from A.A. Lebedev // *Semicond. Sci. Technol.* **21** (2006) R 17, (c) 2006 IOP Publishing Limited.

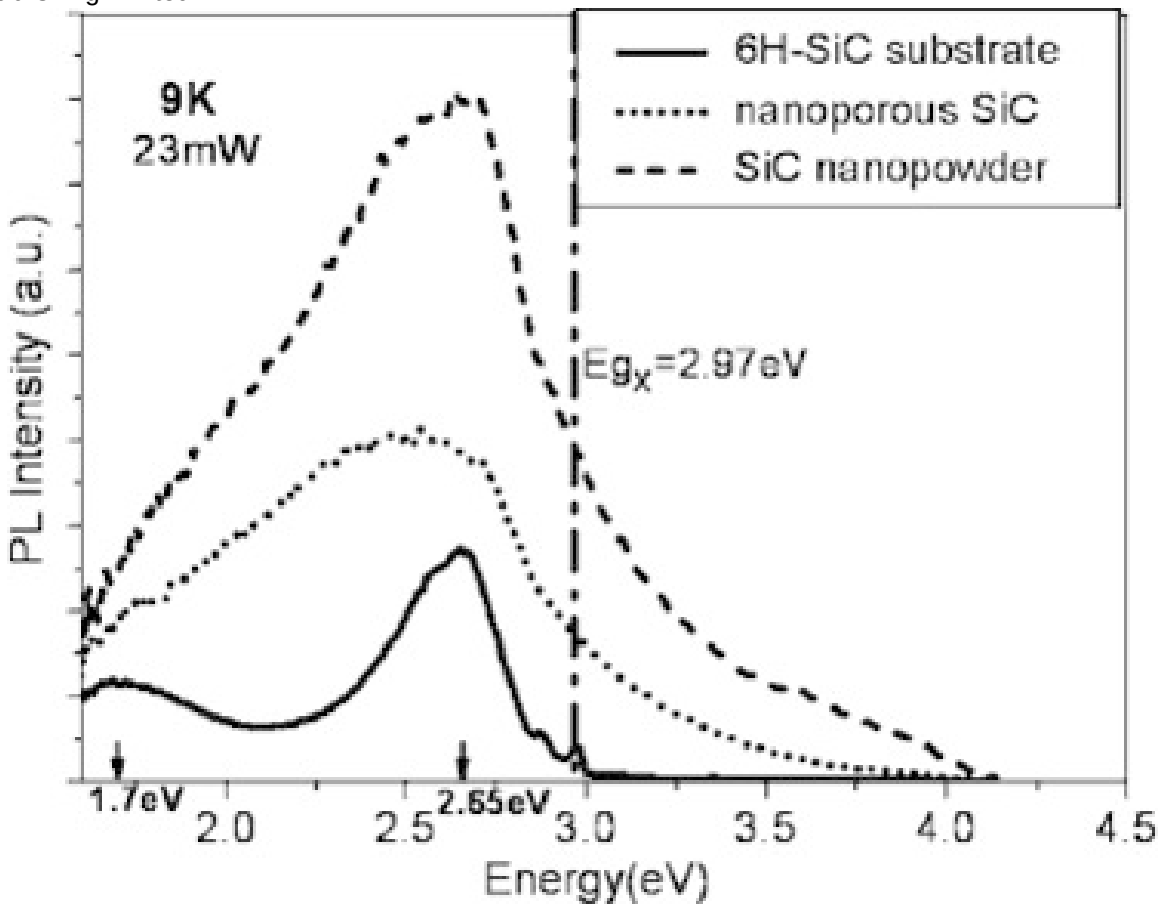

Fig. 2. PL spectra of 6H-SiC wafer (1); nanoporous SiC layer (2), prepared by anodizing of a wafer; and SiC nanopowder (3), made by a strong mechanical grinding of the nanoporous free layer [15]. PL measurements (T = 9K) were performed using a laser line at 5.08 eV from a frequency doubled Ar^+ laser for the exitation was measured. E_{Gx} is the band gap for 6H-SiC. Reprinted with permission from J J. Botsoa, J.M. Bluet, V. Lysenko, O. Marty, D. Barbier and G. Guillot // *J. Appl. Phys.* **102** (2007) 083526; (c) 2007 American Institute of Physics.

4H-SiC polytypes with high density of stacking faults and small amount of 2H and 3C phases. The size effects have been observed in photoluminescence (PL) spectra.

However, these results and other similar those are only continuations and/or some specifications of investigations (carbothermal synthesis, plasma chemistry, laser synthesis, etc.) realized earlier and reflected in reviews [4,5]. Now the primary attention of researchers is focused on preparation of nanosized SiC inclusions in matrixes and of nanowires/nanotubes as perspective materials for opto - and nanoelectronics (light emitting diodes, sensors, etc.) as soon as also porous ceramics for high-temperature filters and catalytic supports. The following basic technological methods are considered: electrochemical and chemical etching, carburization of silicon and silica, implantation of carbon ions in silicon and joint implantation of ions of carbon and silicon in SiO_2 matrixes. These methods as applied to nanosized silicon (as a material for nanoelectronics) were presented in book [13]. The nanosized SiC synthesis methods as applied to electrical/optical properties were discussed by results up to 2005 in review [14] with a comprehensive description of technological regimes.

By analogy with nanosized silicon [13], the PL SiC spectra increase in nanoporous conditions is also observed. Fig. 2 shows low temperature PL spectra for 6H-SiC substrate, nanoporous SiC layer and SiC nanoparticles by the size less than 10 nm [15].

From these data the considerable PL increase for two last subjects and especially for isolated nanoparticles is clearly evident. This phenomenon is connected with the quantum confinement effect. It is considered also that the appreciable contribution in the PL increase is brought by defect structure on the nanopore surface that is formed at etching [14].

Electrochemical anode etching is carried out at a current density of 210 mA/cm^2 in solution HF:C_2H_5OH (1:1) during 25 min [15]. For the detachment of a porous layer (a thickness near by 100 μm) from a substrate the current density quickly increases to 1 A/cm^2. It is also reported about the possibility of refinement of usual 3C-SiC powder (the particle size of some micrometers) to nanoparticles by the size a little nanometer by chemical etching in mix HNO_3:HF (1:3) at 100 °C within an hour with the subsequent centrifugation, washing and so on [16].

Fig. 3 displays the TEM image of SiC (including high resolution TEM (HRTEM) image of one nanocrystal) and the histogram of their distribution in the sizes [16]. Apparently, synthesized nanoparticles are nearly spherical with a diameter ranging from 1.5 to 6.5 nm (the average size of 3.75 nm.), and the picture of the high resolution testifies about high crystalinity with the lattice fringes corresponding to the {111} plane of cubic polytype 3C-SiC. A little agglomeration of the nanoparticles has been also pointed.

At preparation of porous SiC samples the processes of carbide synthesis and formations of a porous skeleton are usually combined, that allows to considerably lower temperature of realization and to organize nanoporous structure. So, heating of the silicon powder mixes with fullerens or with soot in Na steams (promoting mass transfer) at temperature ~700 °C allows to synthesize β-SiC with porosity about 70%. The pore size distribution was in the range of 2-10 nm and grain size was in the nanometer interval also [17]. Nanoporous silicon carbide materials can be also prepared by the polycarbosilane pyrolysis with and without the addition of an inert filler (nano- and microsized SiC powders) [18]. Porous materials-based SiC nanowires (diameter of ~100 nm) with honeycomb structure are reported to prepare by carbothermal reduction of silica [19].

The carbidization study of porous silicon, prepared by electrochemical etching, has revealed the 3C-SiC nanocrystals formation with the size of 5-7 nm at temperature 1200-1300 °C [20]. It is supposed also that due to the mechanism features, a heterostructure is formed including Si nanocrystals and nanosized amorphous SiC particles.

In a number of works (see, for example, [14,21-23]) the features of the SiC nanoparticle implantation (ion beam) synthesis are investigated. In one of the first studies [21] it has been established that implantation of carbon ions with an energy of 50 keV and a dose of 10^{17} sm^{-2} in a silicon substrate with the subsequent thermal annealing and electrochemical etching is accompanied by the occurrence of β-SiC nanocrystals and origin of a new PL peak at about 445 nm (2.79 eV; see also Fig. 2). This new PL peak is 2.7 times as stronger than that of the annealed and etched wafer without implantation. The effect of the ion implantation doses and temperature/duration annealing on structure and optical properties of SiC synthesized nanoparticles is investigated including a separate implantation by carbon or silicon ions, and consecutive double implantation by these ions with use as a substrate of SiO_2 films [14,23]. In last case according to electron paramagnetic resonance (EPR),

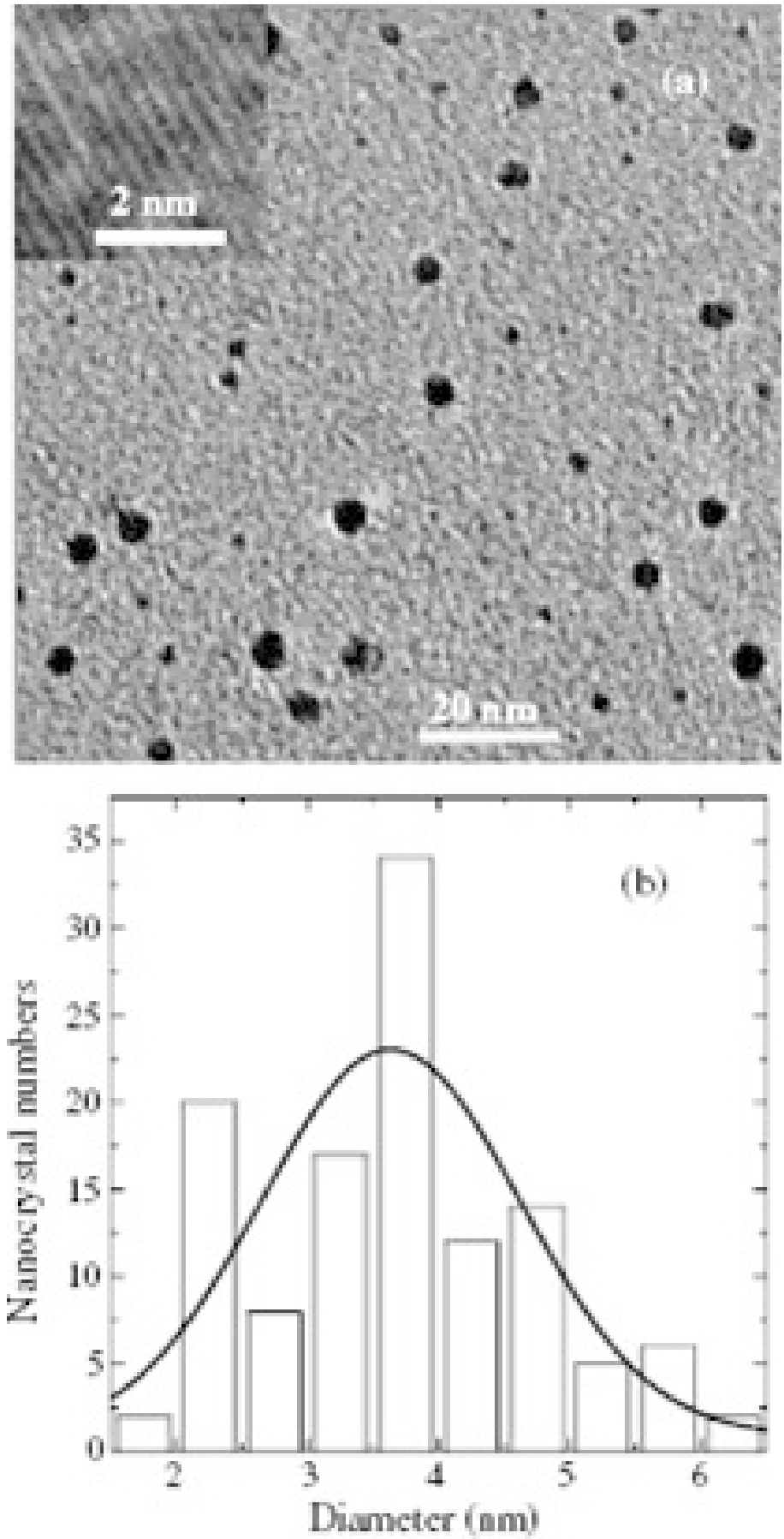

Fig. 3. (a) Brightfield TEM image of the 3C-SiC nanoparticles suspended in ethanol. The inset shows the HRTEM image for one nanoparticle. (b) The histogram of the nanoparticle size distribution [16]. Reprinted with permission from J. Zhu, Z. Liu, X.L. Wu, L.L. Xu, W.C. Zhang and P.K. Chu // *Nanotechnology* **18** (2007) 365603.; (c) 2007 IOP Publishing Limited.

Table 2. Characteristics of SiC nanowires [25-27].

Characteristic	Authors		
	J. Chen et al. [25]	J. Wei et al [26]	F.-L. Wang [27]
Processing duration (h)	4-9	2	1
Diameter (nm)	~200	50-200	60-100
Length (mm)	10-20	Several tenth mm	Several mm
Section shape	Hexagonal	Hexagonal	Roundish
Phase content	β-SiC *a* = 0.4353	β-SiC Traces of *a*-SiC, C and O SiO_2-shell	β-SiC *a* = 0.4370 nm SiO_2-shell
PL presence	n/d	Peaks at 289 nm and 391 nm	n/d

XRD, XPS, PL spectra, HRTEM, scanning electron microscopy (SEM) and other methods, the nanoinclusion formation after implantation and additional annealing is noted. The identification of formed phases and understanding of the got results with revealing of the mechanism of the SiC nanocrystal/amorphous inclusion formation are not so easy and need further investigation.

Implantation of silicon ions (a dose in the range of 10^{16}-2 10^{17} sm^{-2}, energy 40 keV) in carbon nanotubes was investigated in work [24]. Detailed studying of structure and content of the implanted tubes by HRTEM, XRD and energy-dispersive spectroscopy (EDS) has fixed formation of amorphous SiC for which crystallization it is required additional annealing.

Some studiess of the SiC nanowires synthesis on the basis of direct interaction of silicon (or its monoxide) with carbon (see, for example, [25-28]) are known. Reactions set on which synthesis SiC is carried out can be written down by the following way for different variants of interaction [25,27,28]:

$$2C_S + O_2 = 2CO, \quad (1)$$

$$2Si_G + O_2 = 2SiO_G, \quad (2)$$

$$SiO_G + 2C_S = SiC_S + CO, \quad (3)$$

$$SiO_G + CO = SiC_S + O_2, \quad (4)$$

$$3SiO_G + 3C_S = 2SiC_S + SiO_{2(S)} + CO_2, \quad (5)$$

$$SiO_G + 3CO = SiC_S + 2CO_2, \quad (6)$$

$$CO_2 + C_S = 2CO, \quad (7)$$

$$3SiO_G + CO = SiC_S + 2SiO_{2(S)}, \quad (8)$$

$$4CO + 6Si_S = 4SiC_S + 2SiO_{2(S)}. \quad (9)$$

Some of these reactions promote the CO, SiO and SiO_2 reproducibility. The realization of that or other reactions scheme depends on temperature and level of supersaturation but practically they have not studied in detail.

It is noticed that the SiC nanowires preparation is possible by evaporation at 1600 °C in argon atmosphere using different initial products: silicon in graphite crucible and a graphite substrate (reactions (1-4)) [25], a mix of powders of silicon and graphite activated by grinding [26] and mix of powders of silicon monoxide and soot activated by plasma processing (reactions (5-8)) [27]. Table 2 presents comparison of these studies results carried out practically simultaneously at three Chinese universities and focused on large-scale synthesis.

All technological processes are spent without participation of catalysts, i.e. the most probable mechanism of crystal growth can be represented by the scheme of *vapor - solid* (without participation of a liquid phase). The growth direction of crystals is along [111] direction. Fig. 4 shows a general view of SiC nanowires having hexagonal (a and b) and roundish (c) profile. In case of Figs. 4b and 4c, the SiO_2 shell presence is observed (on structural data, the SiO_2 shell is in an amorphous state).

From Table 2 and Fig. 4 it is quite obvious that initial products make considerable impact on the synthesis process but it is difficult to make a pref-

Table 3. Some examples of magnetron sputtering and CVD processing.

Deposition methods. Authors.	Annealing temperature (°C)	Phase content	Grain size, (nm)	Test method
Reactive magnetron sputtering with using Si/C targets (Si substrate) [32]	1100	β-SiC	7.3±0.4 3-10	XRD HRTEM
The same (ion energy of ~90 eV; temperature deposition 700-1050 °C; Si, Al_2O_3, Mo, SiO_2 substrates) [33]	950 1140	80% β-SiC 85%(α+β)-SiC	8-10 17	XRD XPS
Reactive magnetron sputtering in a plasma of (H_2+Ar) at 200-600 °C (Si substrate) [35]	–	β-SiC	4-5	HRTEM
Plasma Enhanced CVD in (CH_4/SiH_4/Ar) gases on Si/SiO_2 substrates at 350 °C [36]	1300	2H-SiC+4H-SiC	15 5	HRTEM XRD
Hot-Mo wire CVD using (SiH_4/CH_4/H_2) gases at 104-434 °C [37]	–	3C-SiC	6-12	XRD

erable choice inconveniently because the data on composition and properties of an end-product while are limited.

Ni catalyst usage results to decrease the temperature of 1050-1100 °C for the 3C-SiC nanowire formation at the CO interaction with the SiO_2/Si interface (reaction (9)) [28].

Synthesis of SiC nanotubes also can be carried out by various methods, for example, at interaction of SiO vapor with carbon nanotubes (at 1200 °C within 100 hour.) [29] or reduction of methyltrichlorosilane by hydrogen in the presence of the catalyst and cocatalyst (ferrocence and thiophene) at temperature 1000 °C during 1 hour [30]. Outer diameter of nanotubes was about 20-80 nm, the value of inner diameter fluctuates in the range of 15-35 nm [30]. The detailed thermodynamic analysis of the β-SiC gas-phase deposition using methyl-trichlorsilane as precursor, has been realized in work [31], in which it was shown that optimum temperature of reduction by hydrogen for the b-SiC preparation is about ~1200 °C.

2.2. Films and bulks

Gas-phase deposition is used for the nanosized SiC film preparation in the known different physical (PVD) and chemical (CVD) versions such as reactive magnetron sputtering, nonreactive magnetron sputtering, hybrid laser-magnetron synthesis, pulsed laser synthesis, plasma enhanced CVD, hypersonic plasma particle deposition, helicon wave plasma CVD, photoassisted CVD, low pressure CVD, and other processes (see, for example, only some recent papers [32-41]). Besides, methods of sublimation and molecular-beam epitaxy are known also. The ammonia addition to the (SiH_2+C_2H_2) precursor results to the SiC films doped by nitrogen [39]. The compositional diamond/β-SiC film deposition is realized by change of (H_2+CH_4+$Si(CH_3)_4$) gas mixture at a microwave plasma enhanced CVD technique [41].

Table 3 shows some examples of magnetron synthesis and CVD processing. Discussing these data, first of all it is necessary to notice that in overwhelming majority of cases the freshly deposited SiC films are amorphous objects and for their transition in a crystal condition it is required either substrate rise in temperature or an additional annealing. Fixing of a structural condition of films is carried out usually by XRD, TEM, FTIR, Raman spectra, XPS, and other methods. The film content characterization is realized by XPS, EDS, Auger electron spectroscopy, Rutherford back-scattering spectroscopy, electron energy loss spectroscopy, and so on.

Fig. 5 shows some examples of temperature evolution of XRD, Raman, and FTIR spectra for SiC films prepared by methods of magnetron sputtering in a plasma of Ar [32], magnetron sputtering in a plasma of H_2+Ar [35] and hot-Mo wire CVD in

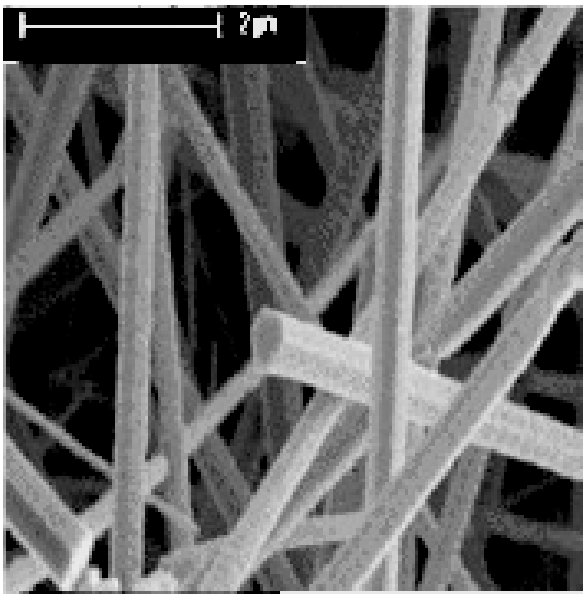

a

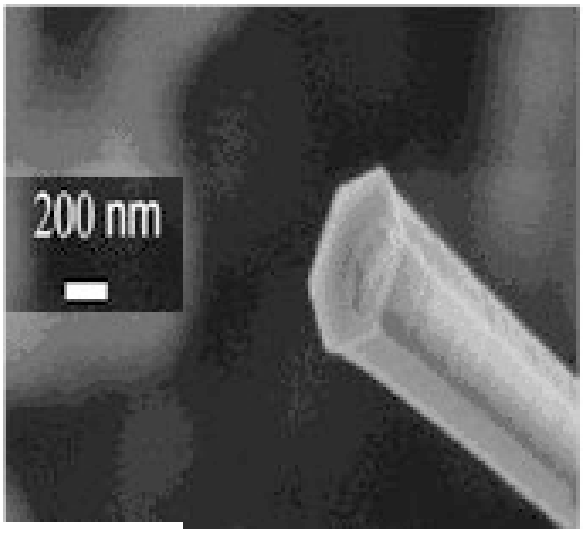

b

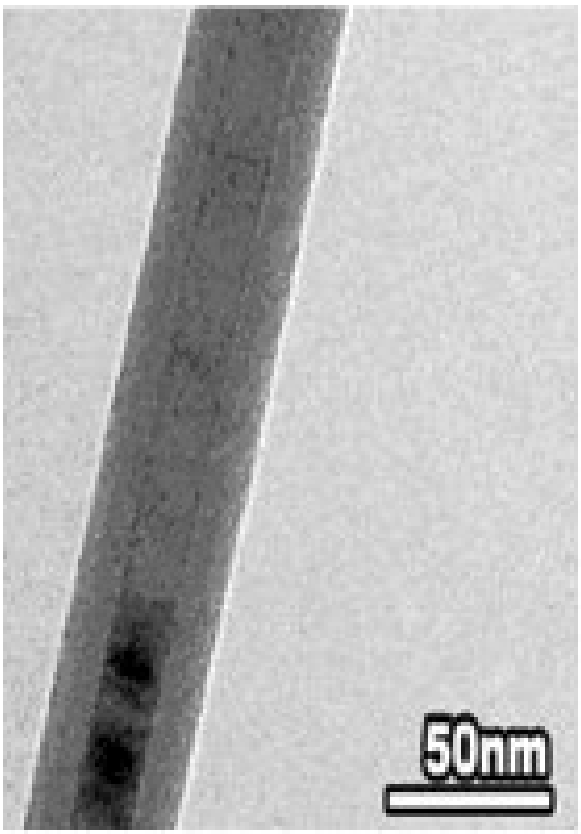

c

Fig. 4. Typical SEM images of SiC nanowires.

the presence of SiH_4, CH_4, and H_2 gases [37]. Temperature conditions of crystallization of those or other SiC polytypes all are various and depend on experimental conditions and many kinetic parameters. There are the different characteristics of various temperature dependences of crystallite growth (for example, non-monotone change with a maximum at 280 °C for tests [37], monotonous that with temperature growth [33] and unthermal that in an interval of 200-600 °C in experiments [35]). All it testifies to necessity of the further continuation of studies.

Recently the method of the solid-state epitaxy of SiC film on silicon consisting in processing of Si single-crystal by CO (T = 1100-1400 °C, P_{CO} = 10-300 Pa, t =5-60 min.) has been developed [42]. It is considered that this interaction results in the silicon vacancy formation in surface layers and the stress relaxation promotion (the stresses arise because of a discrepancy between SiC/Si lattices). It provides the solid-state epitaxy of SiC films growing on silicon with thickness of 20-100 nm. Fig. 6 shows the Pl spectra of 4H and 3C polytypes.

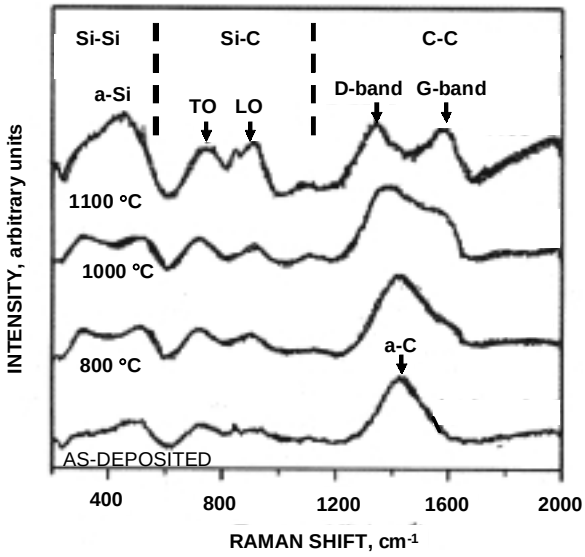

a

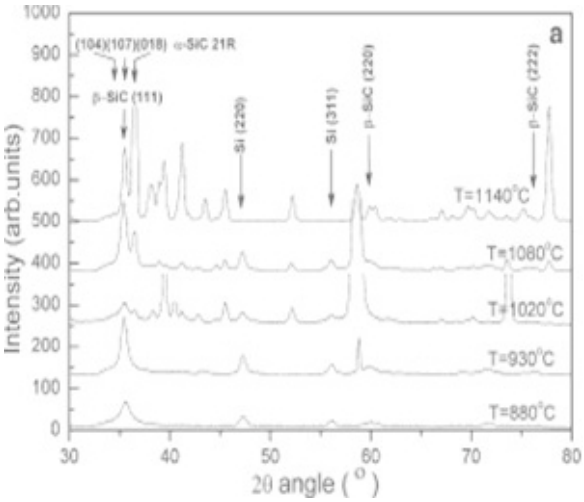

b

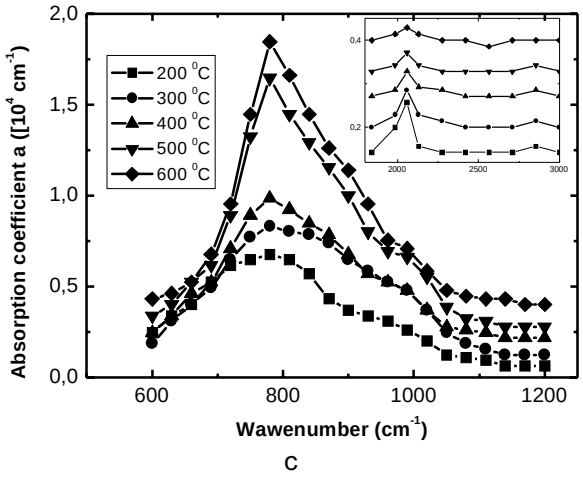

c

Fig. 5. Temperature effect in Raman (*a*) replotted from [32], XRD (*b*) [35], and FTIR (*c*) replotted from [37] spectra of SiC films. In Fig. 5, *a*: a-Si and a-C are amorphous silicon and carbon; TO and LO are transverse and longitude optical modes; D-band and G-band are vibration modes in carbon sublattice. Fig. 5b - reprinted with permission from H. Colder, R. Rizk, M. Morales, P. Marie and J. Vicens // *J. Appl. Phys.* **98** (2005) 024313; (c) 2006 American Institute of Physics.

Liquid-phase epitaxy of 2H-SiC film on a (0001) 4H-SiC substrate in Li-Si melt at 850 °C (*t*=48 hour.) is described in work [43].

In comparison with the SiC nanosized film preparation, attempts of manufacturing bulk nanomaterials are less successful [4,5]. Intensive recrystallization of nanopowders at consolidation temperatures complicates the preparation of bulk nanostructured materials. As applied to nanopowders only using methods of high pressures and high temperatures (sintering at *T*~1200 °C and under pressure of 2-8 GPa) results in making SiC samples with nanograin size [44]. Examples of the dense sample preparation by sintering SiC nanopowders, activated by mechanosynthesis, and high-porous materials by reactive sintering C/Si nanopowders have been described early [4].

3. STRUCTURE AND PROPERTIES

3.1. Structural features and content

Table 4 demonstrates the difference in the stoichiometric coefficients and carbon vacancy concentration for different SiC polytypes [45].

The structure studies of nano-SiC polytypes are not so detailed yet to judge the effect of size factor on a deviation from stoichiometry and vacancy characterization. There are the following values of the cubic SiC-polytype lattice parameter *a* (in nm) such as 0.436 (the grain size of 4-7 nm) [17]; 0.4353 (the nanowire diameter of 200 nm) [25]; 0.4370 (the

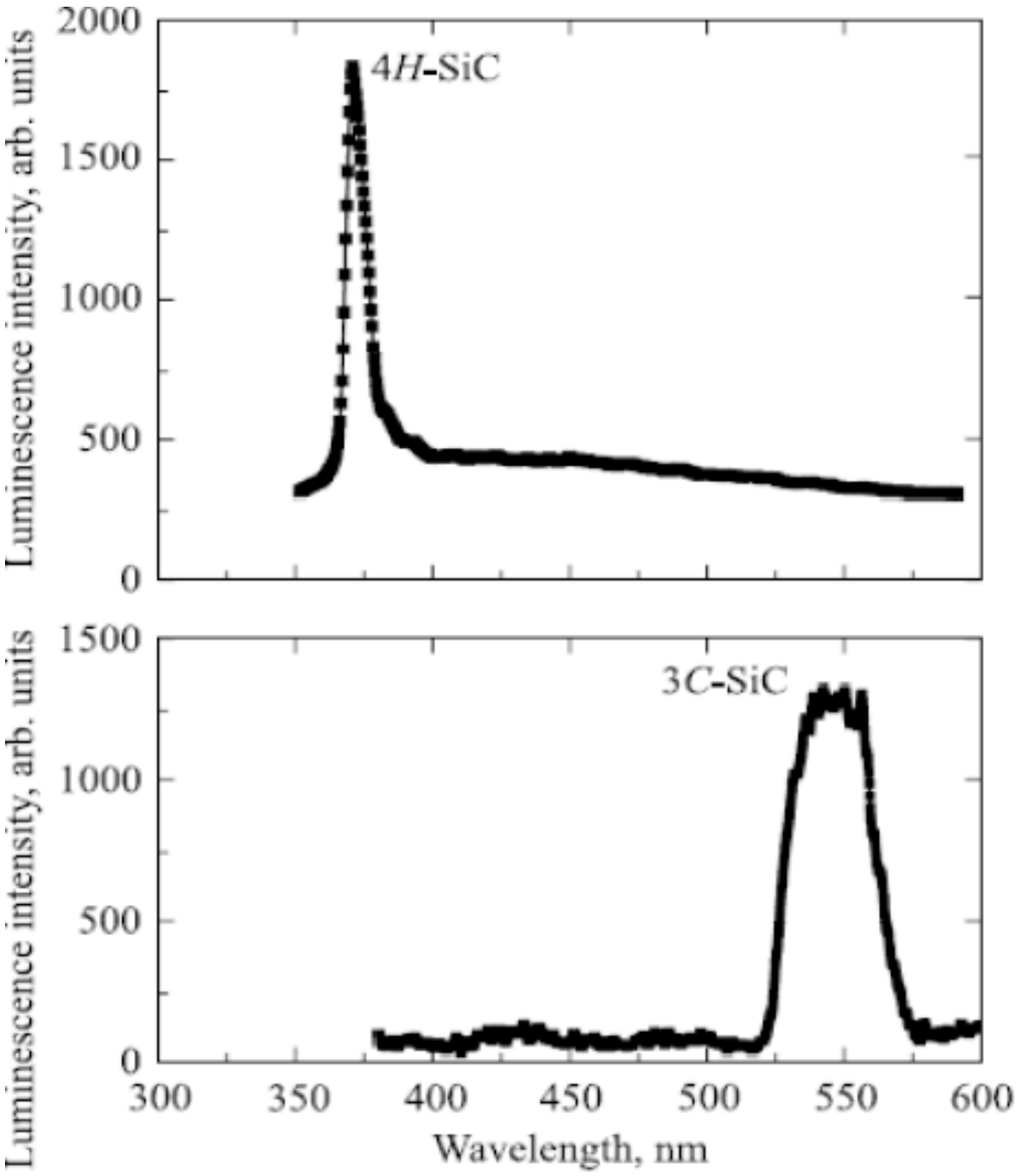

Fig. 6. PL spectra of 4H-SiC and 3C-SiC polytypes (T = 77K) [42]. Reprinted with permission from S.A. Kukushkin and A.V. Osipov // *Phys. Sol. State* **50** (2008) 1238 (English transl.); (c) 2008 MAIK Nauka/ Interperiodika

nanowire diameter of 60-100 nm) [27]; 0.4361 (the nanowire diameter of 60-70 nm) [28]; 0.438 (the grain size of 2-5 nm) [35]. The *a* and *c* values for 6H-polytype are 0.309 nm and 1.525 nm accordingly [35]. These values in the majority are comparable with those given in Table 1; however, it is hard to judge the influence of size effect or impurity content on lattice parameter. Nevertheless, the lattice parameter increase in nanoinclusions of α - and B - polytypes, in comparison with their volume counterparts is marked [35].

Allocation of carbon, argon and hydrogen at the annealing of amorphous and nanocrystalline SiC films was investigated in a number of works (see,

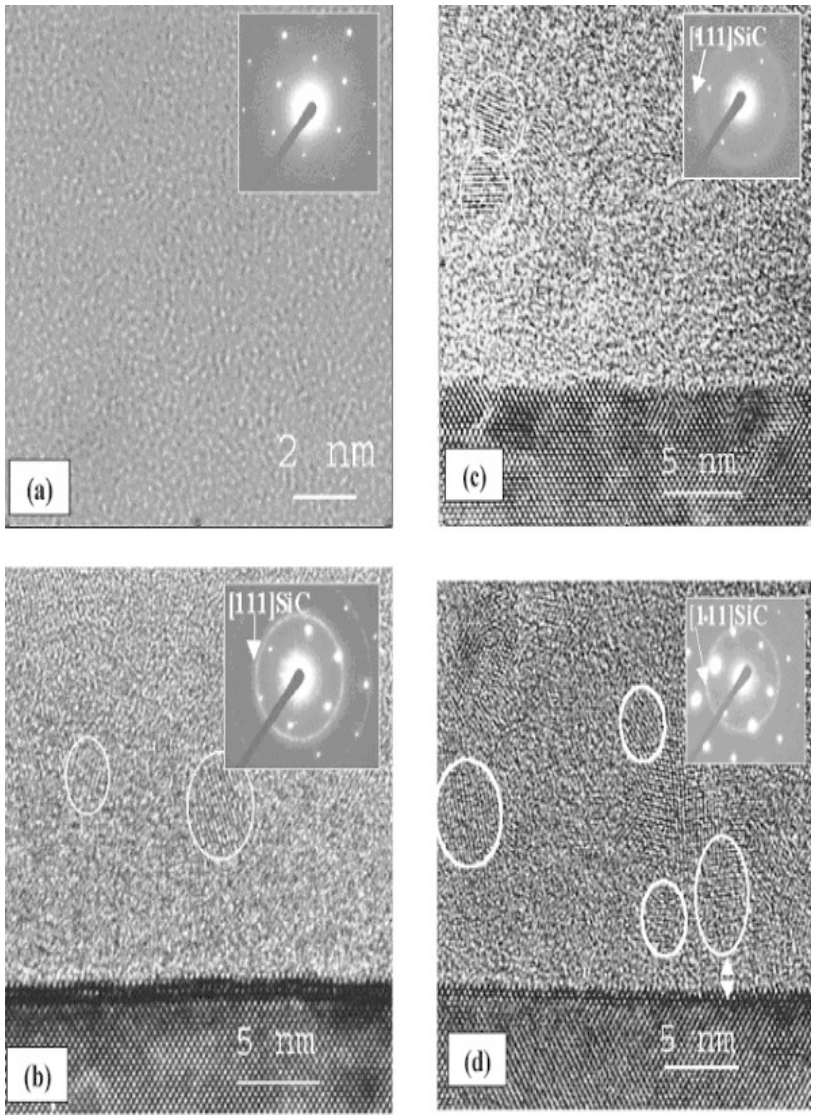

Fig. 7. Cross-sectional TEM micrographs for films deposited at *T*=200 °C (*a*), *T*=300 °C (*b*), *T*=400 °C (*c*), and at *T*=600 °C (*d*) [35]. In the inset, the corresponding SAED patterns. Reprinted with permission from H. Colder, R. Rizk, M. Morales, P. Marie and J. Vicens // *J. Appl. Phys.* **98** (2005) 024313; (c) 2005 American Institute of Physics.

Table 4. Stoichiometry and mean concentration of vacancies in different SiC polytypes [45].

Characteristic	3C	6H	15R	4H
Si/C	1.046	1.022	1.012	1.001
N_C (10^{20} cm^{-3})	33.6	16.3	15.1	7.3

for example, [33,34,36,46,47]). The XRD, HRTEM, FTIR, Raman spectra, XPS methods have allowed to track temperature changes in the Si - Si, C - C and Si – C covalent bonds and reveal the change of content and structure of films. EDS method has revealed the following temperature change of carbon and silicon at the film deposition by electron beam evaporation: 24.18 at .%C and 75.5.65 at.%Si (*T*=500 °C); 17.95% C and 81.12% Si (*T*=1000 °C); 15.20% C and 83.51% Si (*T*=1200 °C) [34]. The silicon excess in these data is connected with the substrate effect; the presence of impurity of oxygen is noted also.

Fig. 7 shows the cross-section sections of HRTEM images of films SiC deposited by magnetron sputtering in Ar/H_2 plasma at different temperatures of silicon substrate [35].

As can be seen from these data (including microdiffraction information on inserts), with increase temperature of the SiC nanoinclusion (6H

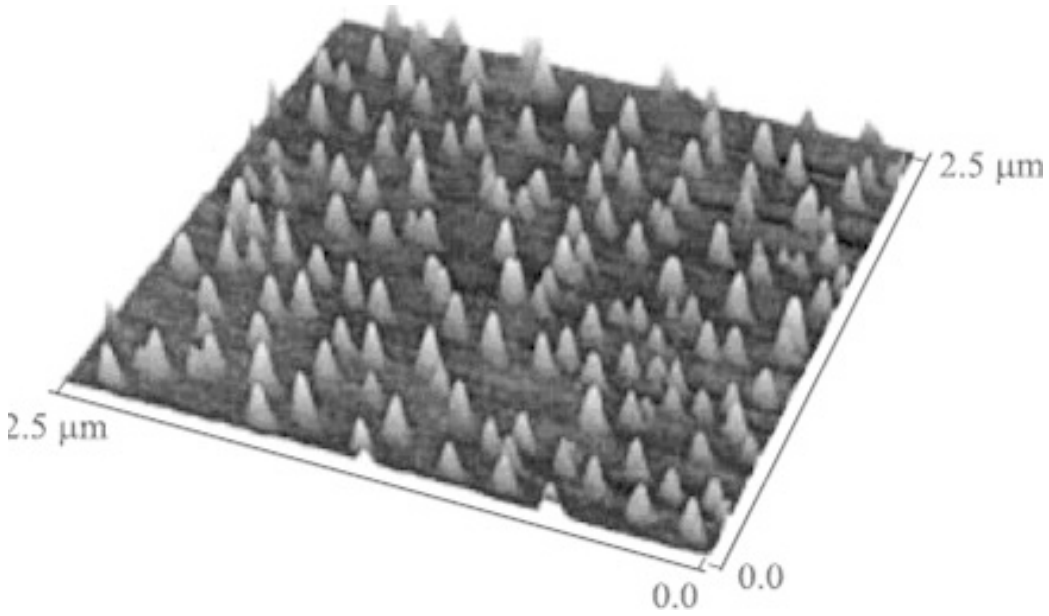

Fig. 8. AFM – image of SiC nucleuses formed by deposition of carbon on Si substrate (the stream of 5 10^{13} cm^{-2} s^{-1}; *T*=925 °C; *t*=10 s). Reprinted with permission from Yu. V. Trushin, E. E. Zhurkin, K. L. Safonov, A. A. Schmidt, V. S. Kharlamov, S. A. Korolev, M. N. Lubov and J. Pezoldt // *Techn. Phys. Lett.* **30** (2004) 641; (c) 2004 MAIK "Nauka/Interperiodika".

or 3C polytypes) crystallization makes progress in an amorphous matrix that is also shown in evolution of IR spectra (see earlier Fig. 5). The analysis of the received information has found out the presence of stacking faults and twins. The analogous situation in the SiC layer deficiencies and presence of stacking faults and twins have been observed in films produced by CVD technology with use of (C_3H_8+SiH_4) precursor [48]. The origin of these planar defects is connected both with features of crystal growth on border of system SiC/Si and with low energy of stacking defects in silicon carbide. The size dependence of twin formation energy in nanosized cubic SiC is analyzed in paper [49].

The porosity and various polytype formation (with their following junction and stacking fault nucleation) was fixed in the case of SiC films prepared by solid-phase epitaxy method [50].

The morphology of growing SiC germs SiC is effectively traced by means of atomic force microscopy (AFM). Fig. 8 shows the example of nucleation after carbon deposition by a method of electron beam evaporation on a Si substrate (111) [51].

These germs have the cone-shaped form with average radius in the basis of an order of 70 nm and average height about 4 nm, their superficial density is about 109 cm^{-2}. The physical model of occurrence and growth of these germs has been developed by the molecular dynamics [52]. Computer simulations of transition time from the two-dimensional growth to three-dimensional one have found out the quite good consent with experimental information.

3.2. Properties

The temperature influence of magnetron sputtering and the subsequent annealing on properties of SiC films (a thickness of 3 mm) is shown in Fig. 9 and Table 5 [47].

The data on properties of sintered and single-crystal SiC samples is given for comparison in Table 5. As already it was marked earlier, SiC films are amorphous in the deposited state. In addition, these films are characterized by the high Ar concentration and significant residual compressive stresses (arising at the expense of the property distinction of a Si substrate and growing layers SiC). From Fig. 9 and Table. 5 it is clear, that with rise in temperature of deposition and the subsequent annealing there is a decrease in the Ar concentration and residual compressive stresses in films as well as an increase of their elastic modulus (*E*) and hardness (H_V). At heating amorphous films gradually

Table 5. Structure, elastic modulus (E) and hardness (H_V) of SiC films prepared by different regimes (T_S – temperature of substrate; T_{ANN} – temperature of additional vacuum annealing with duration 1 hour) [47].

T_S (°C)	T_{ANN} (°C)	Structure (L – grain size)	E (GPa)	H_V (GPa)
25	-	Amorphous	280±5	22.2±0.2
	800	Amorphous	312±6	28.9±0.7
	1000	Amorphous	331±3	34.1±2.1
	1200	Amorphous[a]	365±6	36.3±2.0
400	-	Amorphous	283±5	27.0±0.4
600	-	Amorphous	297±3	30.5±0.4
750	-	Amorphous+β-SiC	378±3	40.0±1.0
	800	Amorphous+β-SiC (L~6 nm)	369±3	39.5±0.5
	1000	Amorphous +β-SiC	374±2	37.8±0.5
750[b]	-	Amorphous+β-SiC (L~3 nm)	385±2	40.5±0.8
	800	Amorphous+β-SiC (L~6 nm)	367±2	40.9±0.8
Coarse-grained sintered SiC			312±7.5	21.6±1.0
Single crystal α-SiC (0001)			499±2.0	36±2.0
Single crystal β-SiC (111)			440±16	32±2.0

a) With signs of nanocrystallization
b) Deposition with bias substrate

Table 6. The effect of grain size (L) of β- SiC on hardness (H_V) and elastic modulus (E).

L (nm)	H_V (GPa)	E (GPa)	Comments
~10	~50	~515	Films deposited by CVD plasma on Mo substrate at ~1200 °C. Fraction of crystalinity of ~85%; residual stresses of ~0.25 GPa [53]
~13	55±10.5	425±84	Films deposited by electron beam PVD on stainless steel at ~900 °C [54]
~20	~37	n/d	Films deposited in supersonic plasma [55]
~70	24-25	n/d	Bulks prepared by hot isostatic pressing of nanopowders [56]

crystallize and, since T~300 °C according to HRTEM (see earlier Fig. 7), the progressive crystallization of b-SiC nanocrystallites (with size of 1-6 nm) is marked. At the same time, the nanocrystallite precipitation was fixed by XRD method only after T~700 °C [47]. Considerable influence on the film properties is rendered also by the negative substrate bias. Thus, an increase of E and H_V indicators is a result of many factors (change of phase structure with an increase of nanocrystallyzation, chemical compound refinement, change of stress state, etc.) and thus it is difficult clearly recognize to differentiate their role.

Comparison of the film hardness and elastic modulus with values for those of conventional macro- and monocrystalline samples shows that the obtained H_V and E characteristics of nano/amorphous films are considerably lower especially in the case of those for single crystal. It is possible to explain this difference by a considerable portion of an amorphous phase in films (their regimes of preparation have not led to full nanocrystallization [47]).

To illustrate a role of size effects in the H_V and E values of nano-SiC it is possible to cite data of other researchers (Table 6).

It is evident that in case of hardness, as well as for other nanomaterials [4,5,58], the decrease of the crystallite size leads to increase of values H_V at the expense of progressive influence of grain

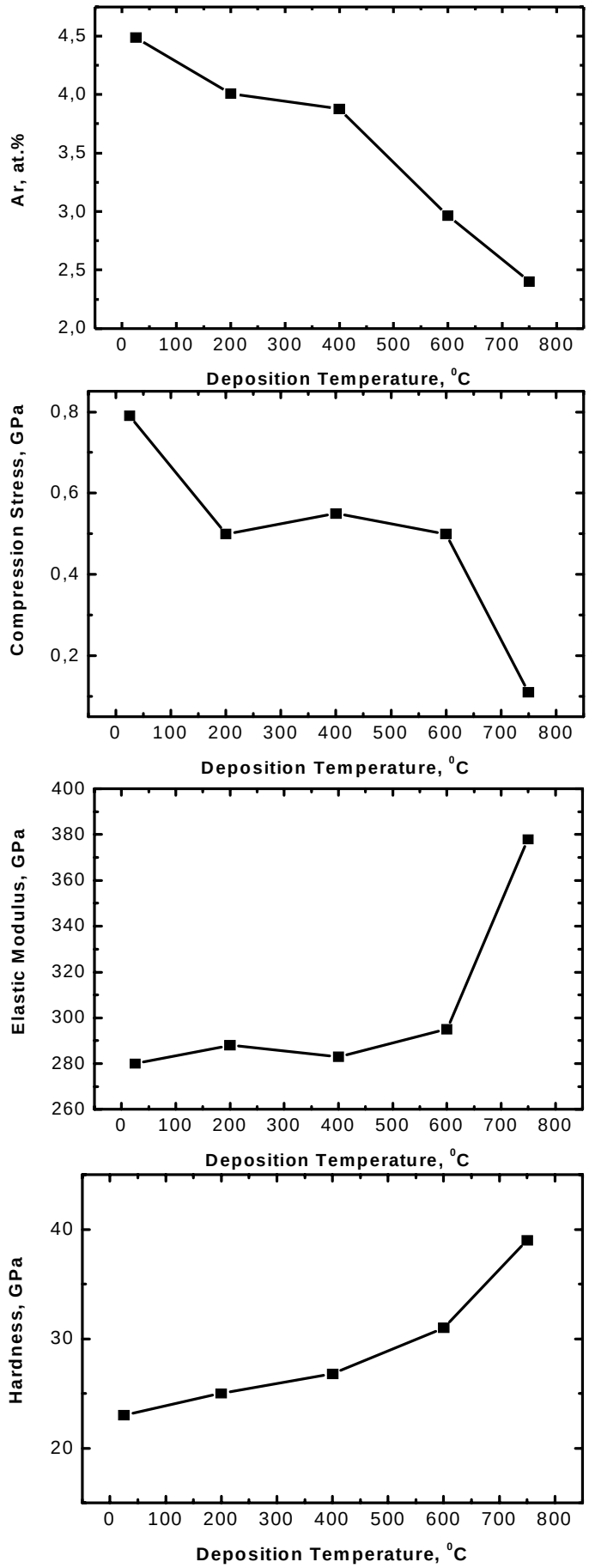

Fig. 9. The hardness, elastic modulus, compressive stresses, and Ar concentration of SiC films as a function of substrate temperature replotted from [47].

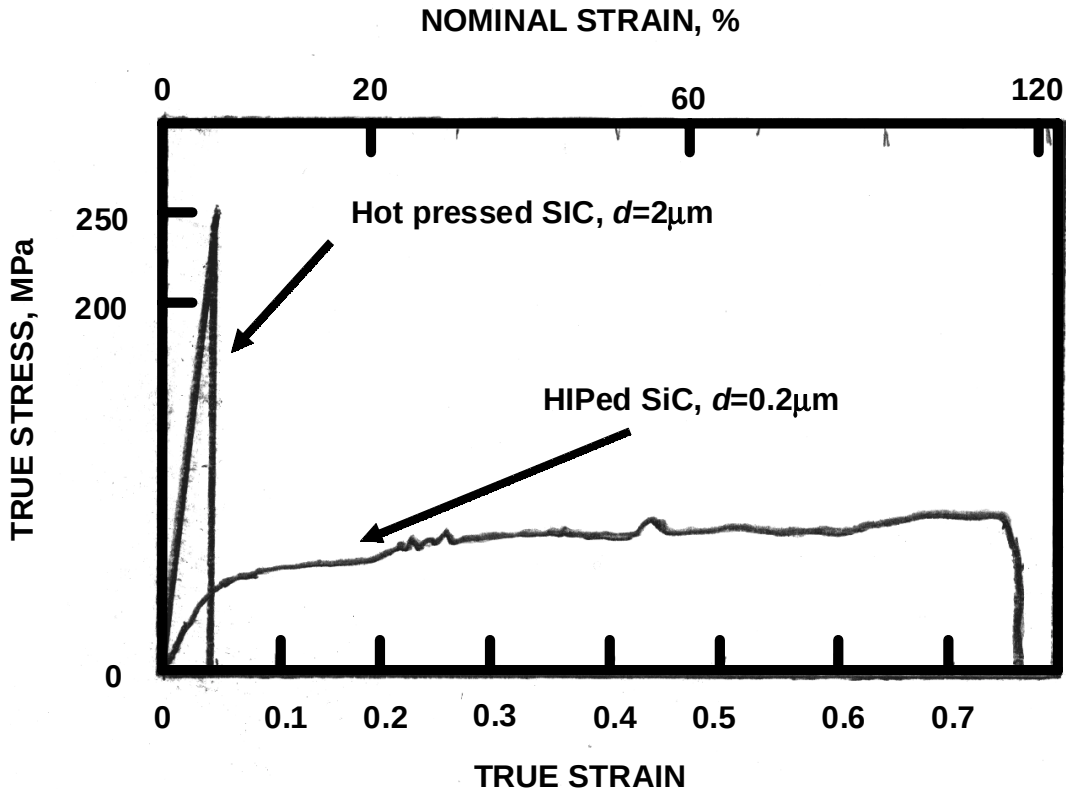

Fig. 10. Behavior at deformation (T=1800 °C, strain rate of 10^{-1} s^{-1}) of β-SiC specimens prepared by hot pressing (grain size of 2 mm) and hot isostatic pressing (grain size of ~0.2 μm) replotted from [65].

boundaries as strong barriers to distribution of dislocations and cracks. For the elastic modulus this dependence has other character: a decrease in values E is observed at the crystallite size for different materials approximately at level less than 30-50 nm at the expense of the part increase of grain boundaries which elastic characteristics are lower in comparison with those for regular crystal state [58]. In the general view, the nano-SiC properties should depend not only from the crystallite size but also from the structure crystallinity, i.e. part in it an amorphous component, and also the specific properties and structure of these components. It is accepted to analyze also properties nano/amorphous SiC composites comparing them with the relation sp^3/sp^2 the carbon configurations taken from Raman spectrometry and XPS and meaning that sp^3 – the configuration corresponds to diamond, and sp^2 – one is to amorphous carbon (see, for example, [54,55]). In the light of told quite clearly that the establishment of dependences $H_V = f(L)$ and $E = f(L)$ for SiC nanomaterials with allocation of a part of the different factor influence requires the further studying. Nevertheless it is quite obvious that there is an essential hardness increase with reduction of the size of grain for SiC as well as for other high-melting point compounds [4,5]. It is noticed also that preliminary results testify in the some increase of fracture toughness (K_{IC}): for films β-SiC with the grain size of 10-15 nm (the width of grain boundaries of 1-2 nm): for usual coarse-grained SiC materials the K_{IC} value is about 2-6 $MPa^{1/2}$ and this indicator for nanostructured SiC films is of 9.2±2 $MPa^{1/2}$ [54,57].

The problem of the strength of brittle nanomaterials-based SiC and other high-melting point compounds is investigated theoretically in frameworks of physics and mechanics of a solid state (see, for example, [58-61]). Such questions as homogeneous and heterogeneous formation of dislocations, origin and movement of cracks on grain boundaries, grain boundary sliding and so on were analyzed.

It is necessary to consider as the most interesting experimental result the observation *in situ* of plastic deformation at the β-SiC (Ø70-100 nm) nanowire testing in HRSEM and HRTEM [62,63]. The testing temperature was close to room and

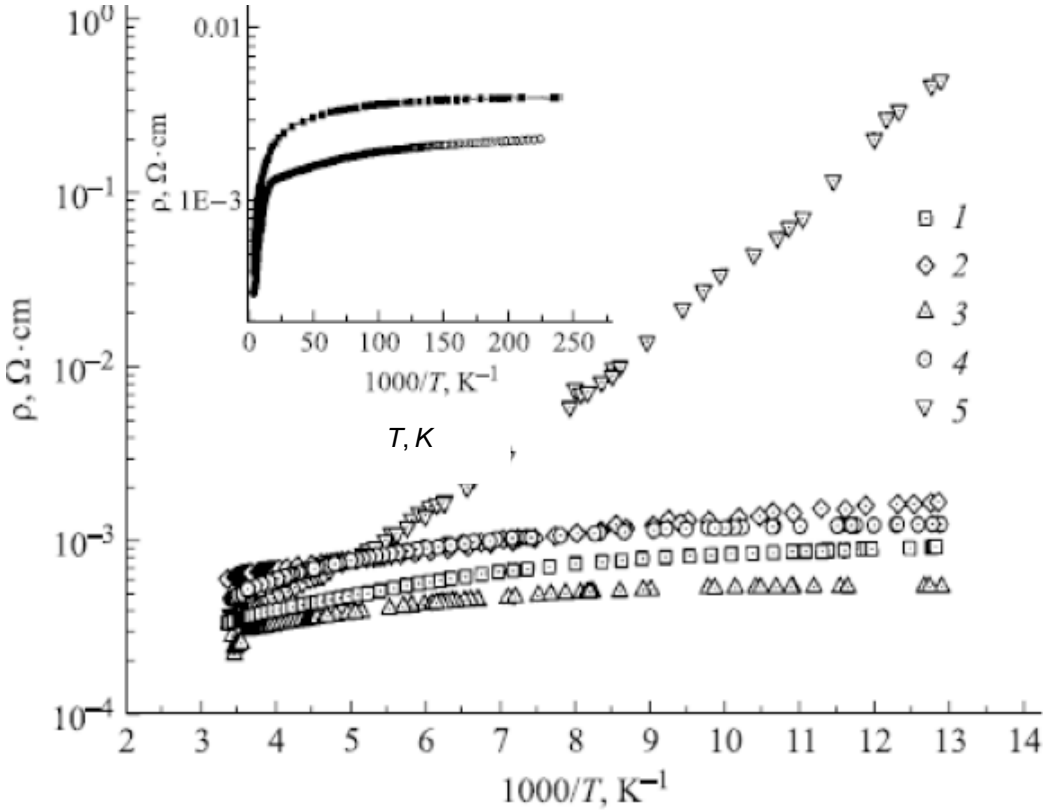

Fig. 11. The temperature effect on electrical resistance 3C SiC/6H SiC heterostructures: 1-4 – heterostructures with different level of alloying layer 3C; 5 – substrate 6H. In the inset, the temperature dependence for heterostructures in low-temperature interval. Reprinted with permission from A. A. Lebedev, P. L. Abramov, N. V. Agrinskaya, V. I. Kozub, A. N. Kuznetsov, S. P. Lebedev, G. A. Oganesyan, L. M. Sorokin, A. V. Chernyaev and D. V. Shamshur // *Techn. Phys. Lett.* **33** (2008) 1035; (c) 2008 MAIK "Nauka/Interperiodika".

deformation made more than 200%. An increase of dislocation density at an initial stage and structure amorphization at a final stage were fixed. It is necessary to note the results of computer experiment (the model with the sizes of 62.5×62.5×53.5 nm^3 contained 18.7 million atoms; the grain size was of 8 nm) in which the presence of grain boundary slidings at the first stage of deformation and the subsequent transgrain dislocation shears have been revealed at a room temperature [64].

The deformation behavior (T=1800 °C) of β-SiC samples with the grain size of ~2 mm and ~0.2 mm is shown in Fig. 10 [65]. It is evident that this is a typical brittle deformation for coarsegrain samples and the objects with structure close to nanostructure find out superplasticity (deformation of ~110 %).

Pertinently to underline that as a rule the temperature of brittle-plastic transition for usual coarse-grained β-SiC samples is not lower 900°-1200 °C [66] (by data of Fig. 10 even more 1800 °C) i.e. a decrease of this characteristic can be considerable enough in the case of transition to nanomaterials but the realization of this advantage is very hard for massive (bulk) nanosubjects as the technology of their preparation should provide the high nanostructure perfection with an exception of nano - and microporosity and other defects both in nanograins and especially on their grain boundaries.

Let us consider the characteristic of the nano-SiC physical properties. Earlier in Fig. 2, by data [15], evolution of PL spectra for 6H-SiC at transition from coarse-grained substrates to nanoporous sample and isolated nanoparticle was already shown. Many examples of similar changes of luminescence and optical properties of nano-SiC (on an example of nanoparticles, nanowires,

nanotubes, nanofilms, and quantum points) with the analysis of theoretical results are resulted in review [14]. The theory of the PL spectra change and widening of band gap in connection with quantum-dimensional effect (quantum confinement effect) is based on the analysis of band structure taking into account finiteness of the nanocrystallite size. As it is known that energy of electronic excitation in nanosemiconductors surpasses energy of band-to-band transition in corresponding macroscopic semiconductors. With reference to nano-Si it is in detail described in monograph [13]. Proceeding from theoretical estimations, the widening of band gap for hexagonal polytype 6H-SiC begins at radius of nanosubjects less than ~7 nm (an abrupt ascension since the sizes of <3 nm); for cubic polytype 3C-SiC these sizes make accordingly of <4 nm and of <1.5 nm [14]. Most full theoretical and experimental studies were carried out for cubic polytype in which the value of the band gap for diameters of 3.9 nanometers and 8.8 nanometers have appeared ~2.7 eV and ~2.3 eV correspondingly (last value is close to tabular that – see Table 1) [67].

The optical properties, chemisorption characteristics and stability of SiC nanotubes (in various forms depending on their geometrical sizes and chirality) have been estimated theoretically from the first principles – *ab initio* [68-71]. For example, it is shown that NO_2 molecules can be chemisorbed on SiC nanotubes in contrast with either carbon nanotubes or boron nitride those.

Study of electrical and galvanomagnetic properties of amorphous SiC:H films and epitaxial 3C-SiC films has been undertaken in papers [72,73]. Effect of annealing of amorphous films on their conductivity resulted in the reveal of the activation energy temperature dependence [72]. The temperature dependence of the 3C-SiC film specific electrical resistance on a substrate 6HSiC is shown in Fig. 11 [73].

Apparently from these data, is shown that with temperature fall the heterostructure 3C-SiC/6HSiC electrical resistance (ρ) increases gradually on the exponential law and at T<50K this change is proportional to $T^{1/3}$. At temperature of liquid nitrogen (77K) the ρ value of a substrate (hexagonal polytype) is approximately on 2 order above than the ρ value of films. The studied epitaxial layers possessed conductivity of n-type; concentration of carriers and their mobility at 300K made 2 10^{18} cm^{-3} and 40 cm^2/V sec and that is close enough to tabular data (see Table 1). The analysis of results has shown also that low resistance of these layers at helium temperatures can be connected with transition from insulator to metal.

Data on electrical and optical properties of 3C-SiC/6H-SiC heterostructures and superlattices (multilayered films) on their basis with reference to electronics problems are generalized in review [7].

Recently works on research of the irradiation influence on properties of nano-SiC have begun. The comparison of structural evolution of samples 3C-SiC in a usual crystal condition (the grain size of ~1 μm, porosity of 15%) and with nanostructure (the grain size of ~36 nm, porosity of 8%) has shown that the irradiation at a room temperature by ions Xe (energy 95 MeV; dose 5×10^{14} sm^{-2}) is accompanied approximately by identical changes of the cell parameter and does not lead to the structure amorphization [74]. While the irradiation of the monocrystalline 6H-SiC at room temperature with low energy ions resulted in the total amorphization. The change of PL, IR, XRD, and Raman spectra after joint implantation of C and Ca ions in 6H-SiC thin films is analysed in paper [75].

Encouraging results of the biological property study of amorphous SiC films with reference to biomedical applications are marked in a number of works (see review [76] and Refs. in it). Tests *in vivo* and *in vitro* have revealed, for example, that the SiC biocompatibility with cages of the animal organisms possessing ability to grasp and digest alien particles (phagocytosis). However, an accumulation of regular data on the nano-SiC biological characteristics only begins. It is especially important in connection with known risks concerning toxicity of nanosubjects.

4. CONCLUSIONS

The investigation of the nano-SiC properties has revealed many interesting results among which first of all we will note the possibility of the hardness essential increase, display of the nanowire high plasticity, substantial increase of the PL spectra intensity, biocompatibility, good resistance to amorphization under irradiation and some other. Traditional scopes of the SiC material application (such as abrasives, refractories, heaters, some semiconductor devices, additives to composites, nanosized powders, etc.) have received a good impulse to potential expansion. The high biological compatibility and wear resistance of nano-SiC made these materials perspective as coverings for the implanted microelectrodes and the worn out joints as well as in high-porous membranes and biosensors [76]. Chemical inertness and

biocompatibility in connection with optical properties open the possibilities of the SiC quantum points using for fluorescing diagnostics in medicine [77]. The prospects of these materials in opto – and nanoelectronics [7,78], in MEMS and NEMS systems it is quite obvious [79,80] as well as for porous high-temperature filters and catalyst supports [17,19]. High radiation resistance of SiC nanomaterials makes them very perspective as an important candidate for the nuclear fusion reactors like ITER and high-temperature gas cooled reactors [74,81]. It is also important to take attention to the novel hard amorphous nanocomposite Si-B-C-N coatings with oxidation resistance above 1000 °C [82].

The realization of listed applications substantially depends on efficiency of the nano-SiC manufacturing technology method. Here pertinently to note a method working out the solid-state epitaxy of SiC film on silicon [42]. It is considered that the layers received thus nano-SiC will find applications as substrates, light-emitting diodes and solar batteries [83]. On the other hand, the possibilities of consolidated bulk nano-SiC materials [84] seems to be more productive in near future. There are some encourage results of spark plasma sintering nanoscale SiC structures [85]. As a result, the necessity of comparison of the nano-SiC manufacturing technology various methods, as it was marked early, is very urgent.

At the same time the lack of data about the stability of physical, chemical, and mechanical properties of these materials and accordingly of their operational characteristics is felt. Certainly, the nano-SiC wide realization demands also the further development of basic researches in the field of dimensional effects.

ACKNOWLEDGEMENTS

The support of the Russian Found of Basic Research (Projects No 08-03-00105 and No 09-03-11000) and the Program of Fundamental Researches of Russian Academy of Sciences (Subprograms P-18 and P-27) is acknowledged. The author is grateful to Mr. V.V. Klucharev, Mrs. S.V. Klucharev, and Dr. A.V. Khatchoyan for their active help in the review preparation as well as to Prof. D.I. Tetelbaum for fruitful discussion.

REFERENCES

[1] *Silicon Carbide 2006 – Materials Processing and Devices. Vol. 911*, ed. by M. Dudley, M. Capano, T. Kimono, A.R. Powell and Sh. Wang (Mater. Res.Soc., Warrendale, 2006).

[2] *Silicon Carbide and Related Materials. ECSCRM 2006. Vols. 556-557*, ed. by N. Wright, C.M. Johnson, K. Vassilevski, I. Nikitina and A. Horsfall (Trans. Tech. Publ. Mater. Sci. Forum, Switzerland, 2007).

[3] *Silicon Carbide 2008 –Materials, Processing and Devices. Vol. 1069*, ed. by M. Dudley, C.M. Johnsohn, A.R. Powell and S.-H. Ryu (Mater. Res. Soc., Warrendale, 2008).

[4] R.A. Andrievski // *Russ. Chem . Rev.* **74 (**2005) 1061 (English transl.).

[5] R.A. Andrievski, In: *Nanomaterials handbook*, ed. by Y. Gogotsi (CRC Press: Boca Raton FL, 2006), p. 405.

[6] R.A. Andrievski // *Nanotechnologies in Russia* **2** (2007) 6 (English transl.).

[7] A.A. Lebedev // *Semicond. Sci. Technol.* **21** (2006) R 17.

[8] L.L. Snead, T, Nozawa, Y, Katoh, T.-S. Byun, S. Kondo and D.A. Petti // *J. Nucl. Mater.* **371** (2007) 329.

[9] S.A. Kukushkin, A.V. Osipov, V.N. Bessolov, B.K. Medvedev, V.K. Nevolin and K.A. Tcarik // *Rev. Adv. Mater. Sci.* **17** (2008) 1.

[10] H. Lin, J.A. Gerbec, M. Sushchikh and E.W. McFarland // *Nanotechnology* **19** (2008) 325601-08.

[11] Y. Leconte, M. Leparoux, X. Portier and N. Herlin-Boime // *Plasma Chem. Plasma Process.* **28** (2008) 233.

[12] A.A. Zhokhov, V.M. Masalov, D.V. Matveev, M.Y. Maksimuk, I.I. Zver'kova, S.S.Khasanov, S.Z. Shmurak, A.P. Bazhenov and G.A. Emel'chenko // *Phys. Sol. State* **51** (2009) 1626 (English transl.).

[13] N.N. Gerasimenko and Yu.N. Parkhomenko, *Silicon – material for nanoelectronics* (Technosphera, Moscow, 2007), in Russian.

[14] J.Y. Fan, X.L. Wu and Paul K. Chu // *Prog. Mater. Sci.* **51** (2006) 983.

[15] J. Botsoa, J.M. Bluet, V. Lysenko, O. Marty, D. Barbier and G. Guillot // *J. Appl. Phys.* **102** (2007) 083526.

[16] J. Zhu, Z. Liu, X.L. Wu, L.L. Xu, W.C. Zhang and P.K. Chu // *Nanotechnology* **18** (2007) 365603.

[17] F. Kawamura, H. Yamane, T. Yamada, Sh. Yin and T.Sato // *J. Am. Ceram. Soc.* **91** (2008) 51.

[18] A.R. Maddocks, D.J. Cassidy, A.S. Jones and A.T. Harris // *Mater. Chem. Phys.* **113** (2009) 861.

[19] J.-S. Lee, S.-H. Lee and S.-Ch. Choi // *J. All. Comp.* **467** (2009) 543.
[20] Y.S. Nagornov, B.M.Kostishko, C.N. Mikov, Sh.R. Atazhanov, A.V. Zolotov and E.S. E.S.Pchelintzeva // *Techn. Phys.* **77** (2007) 135. (English transl.).
[21] L.-Sh. Liao, X.-M. Bao, Zh.-F. Yang and N.-B. Min // *Appl. Phys. Lett.* **66** (1995) 2382.
[22] Y.Z. Wan, G.Y. Xiong, F. Song, H.L.Luo, Y. Huang, F. He, L.B. Guo and Y.L. Wang // *Surf. Rev. Lett.* **14** (2007)1103.
[23] D. I. Tetelbaum, A. N. Mikhaylov, V. K. Vasiliev, A. I. Belov, A. I. Kovalev, D.L.Wainstein, Yu.A. Mendeleva, T.G. Finstad, S. Foss, Y. Golan and A. Osherov // *Surf. Coat. Technol.* **203** (2009) 2658.
[24] H. Liu, G.-A. Cheng, Ch. Liang and R. Zheng // *Nanotechnology* **19** (2008) 245606.
[25] J. Chen, G. Yang, R. Wu, Y. Pan, J. Lin, R. Zhai and L. Wu: // *J. Nanosci. Nanotechnol.* **8** (2008) 2151.
[26] J. Wei, K. Li, H. Li, D. Hou, Y. Zhang and Ch. Wang // *J. All. Comp.* **462** (2008) 271.
[27] F.-L. Wang, L.-Y. Zhang and Y.-F. Zhang // *Nanoscale Res. Lett.* **4** (2009) 153.
[28] G. Attolini, F. Rossi, M. Bosi, B.E. Watts and G. Salviati // *J. Non-Cryst. Sol.* **354** (2009) 5227.
[29] T. Taguchi, N Igawa, H. Yamamoto and S. Jitsukawa // *J. Am. Cearam. Soc.* **88** (2005) 459.
[30] Zh. Xie, D. Tao and J. Wang // *J. Nanosci. Nanotechnol.* **7** (2007) 647.
[31] J. Deng, K. Su, X. Wang, Q. Zeng, L. Cheng, Y. Xu and L. Zhang // *Theor. Chem. Acc.* **122** (2009) 1.
[32] D. Song, E.-Ch. Cho, Y.-H. Cho, G. Conibeer, Y. Huang. Sh. Huang and M.A. Green //*Thin Sol. Film* **516** (2008) 3824.
[33] A.V. Semenov, V.M. Puzikov, M.V. Dobrotvorskaya, A.G. Fedorov and A.V. Lopin *// Thin Sol. Films* **516** (2008) 2899.
[34] M. Jelinek, T. Kocourek, J. Zemek, M. Novotny and J. Kadliec // *Appl. Phys. A: Mater. Sci. Proc.* **93** (2008) 633.
[35] H. Colder, R. Rizk, M. Morales, P. Marie and J. Vicens // *J. Appl. Phys.* **98** (2005) 024313.
[36] M. Kuenle, S. Janz, O. Eibl, C. Berthold, V. Presser and K.-G. Nickel // *Mater. Sci. Eng.* **B,** 159-160 (2009) 355.
[37] A. Tabata, Y. Komura, Y. Hoshide, T. Narita and A. Kondo // *Jap. J. Appl. Phys.* **47** (2008) 561.
[38] S.L. Koeng and O. Shevaleevskiy // *Pure Appl. Chem.* **80** (2008) 2141.
[39] X.-A. Fu, S. Noh, L.Chen and M. Mehregany // *J. Nanosci. Nanotechnol.* **8** (2008) 3063.
[40] A.R. Beaber, L.J. Qi, J. Hafiz, P.H. McMurry, J.V.R. Heberlein, W.W. Gerberich and S.L. Girshick // *Surf. Coat. Technol.* **202** (2007) 871.
[41] V.V.S.S. Srikanth, T. Staedler and X. Jang // *Appl. Phys. A*: *Mater. Sci. Proces.* **91** (2008) 149.
[42] S.A. Kukushkin and A.V. Osipov // *Phys. Sol. State* **50** (2008) 1238 (English transl.).
[43] M. Imade, T. Ogura, M. Uemura, F. Kawamura, M. Yoshimura, Y. Kitaoka, T. Sasaki, Y. Mori, M. Yamazaki, Sh. Suwabe and Sh.-I. Nakashima // *Mater. Lett.* **63** (2009) 649.
[44] A. Swiderska-Sroda, G. Kalisz, B. Palosz and N. Herlin-Boime // Rev. Adv. Mater. Sci. **18** (2008) 422.
[45] A.A. Lebedev and S.Yu. Davidov // *Semiconductors* **39** (2005) 277 (English transl.).
[46] S. Muto and T. Tanabe // *J. Appl. Phys.* **93** (2003) 3765.
[47] V. Kulikovsky, V. Vorlíček, P. Bohač, M. Stranyanek, R. Čtvrlik, A. Kurdyumov and L. Jastrabik // *Surf. Coat. Technol.* **202** (2008) 1738.
[48] E.J. Oliver and J.H. Neethling // *Int. J. Refr. Met. Hard Mat.* **27** (2009) 443.
[49] Y. Zhang, H. W. Shim and H. Huang // *Appl. Phys. Lett.* **92** (2008) 261908.
[50] L.N. Sorokin, N.V. Vesekov, M.P. Scheglov, A.E. Kalmykov, A.A. Sitnikov, A.A. Feoktistov, A.V. Osipov and S.A. Kukushkin // *Techn. Phys. Lett.* **34** (2008) 992 (English transl.).
[51] Yu. V. Trushin, E. E. Zhurkin, K. L. Safonov, A. A. Schmidt, V. S. Kharlamov, S. A. Korolev, M. N. Lubov and J. Pezoldt // *Techn. Phys. Lett.* **30** (2004) 641 (English transl.).
[52] Ę.L. Safonov, *Study of nanocluster nucleation and growth by molecular-beam epitaxy in SiC/C, Ge/Si and InAs/GaAs systems by computer modeling. PhD thesis* (St. Petersburg, Techn. University, Russia, 2009), in Russian.
[53] F. Liao, S.L. Gershick, W.M. Mook, W.W. Gerberich and M.R. Zachariah // *Appl. Phys. Lett.* **86** (2005) 171913.

[54] X. Zhao, X. He, Y. Sun, J. Yi and P. Xiao // *Acta Mater.* **57** (2009) 893.
[55] N. Tymiak, D.I. Iordanoglu, D. Neumann, A. Gidwani, F. Di Fonzo, M.H. Fan, N.P. Rao, W.W. Gerberich, P.H. McMurri, J.V.R. Heberlein and S.L. Girshick, In: *Proc. 14th Int. Symp. on Plasma Chemistry* (Prague, Czechia, 1999), p. 1989 (citing on [54]).
[56] R. Vassen and D. Stover // *Mater. Sci. Eng. A* **301** (2001) 59.
[57] X. Zhao, R.M. Langfold, J. Tan and P. Xiao // *Scr. Mater.* **59** (2007) 39.
[58] R.A. Andrievski and A.M. Glezer // *Physics – Uspekhi* **179** (2009) 315 (English transl.).
[59] M.Yu. Gutkin and I.A. Ovid'ko, *Physical mechanics of deformed nanostructures. Vol. II. Nanocrystalline films and coatings* (Janus, St. Petersburg, 2005), in Russian.
[60] I.A. Ovid'ko, A.G. Sheinerman and E.C. Aifantis // *Acta Mater.* **56** (2008) 2718.
[61] I.A. Ovid'ko and A.G. Sheinerman // *Scr. Mater.* **59** (2008) 119.
[62] X.D. Han,, Y.F. Zhang, K. Zheng, X.N. Zhang, Z. Zhang, Y.J. Hao, X.Y. Guo, J. Yuan and Z.L.Wang // *NanoLetters* **7** (2007) 452460.
[63] Y. Zhang, X. Han,, K. Zheng, Z. Zhang, X. Zhang, J. Fu, Y. Ji, Y. Hao, X. Guo and Z. Wang // *Adv. Funct. Mater.* **17** (2007) 3435.
[64] I. Szlufarska, A. Nakano and P. Vashishta // *Science* **309** (2005) 911.
[65] Y. Shinodu, T. Nagano, H. Gu and F. Wakai // *J. Am. Ceram. Soc.* **82** (1999) 2916.
[66] R.A. Andrievski and I.I. Spivak, *Strength of high-melting compounds and materials on their base* (Metallurgia, Cheliabinsk, 1989), in Russian.
[67] X.L. Wu, J.Y. Fan, T Qiu., X. Yang, G.G. Siu and P.K. Chu // *Phys. Rew. Lett.* **94** (2005) 026102.
[68] I.J. Wu and G.Y Guo // *Phys. Rev. B* **76** (2007) 035343.
[69] S.-P. Huang, D.-S. Wu, J.-M. Hu, H. Zhang, Z. Xie, H. Hu and W.-D. Cheng // *Optics Express* **15** (2007) 10947.
[70] G. Gao, S.H. Park and H.S. Kang // *Chem. Phys.* **355** (2009) 50.
[71] G. Alfieri and T. Kimoto // *Phys. Stat. Sol. B* **246** (2009) 407.
[72] L. Magafas, D. Bandekas, A.K. Boglou and A.N. Anagnostopoloulos // *J. Non-Cryst. Sol.* **353** (2007) 1065.
[73] A. A. Lebedev, P. L. Abramov, N. V. Agrinskaya, V. I. Kozub, A. N. Kuznetsov, S. P. Lebedev, G. A. Oganesyan, L. M. Sorokin, A. V. Chernyaev and D. V. Shamshur // *Techn. Phys. Lett.* **33** (2008) 1035 (English transl.).
[74] A. Audren, I. Monnet, Y. Leconte, X. Portier, L. Thome, M. Levalois, N. Herlin-Boime and C. Reynaud // *Nucl. Instr. Methods Phys. Res. B* **266** (2008) 2806.
[75] Z.C. Feng, S.C. Lien, J.H. Zhao, X.W. Sun and W. Lu // *Thin Sol. Films* **516** (2008) 5217.
[76] R. Yakimova, R.M. Petoral Jr, G.R. Yazdi, C. Vahlberg, A. Lloyd Spetz and K. Uvdal // *J. Phys. D: Appl. Phys.* **40** (2007) 6435.
[77] J. Botsoa, V. Lysenko, A. Geloen, O. Marty, J.M. Bluet and G. Guillot // *Appl. Phys. Lett.* **92** (2009) 173902.
[78] N. G. Wright, A.B. Horsfall and K. Vassilevski // *Materialstoday* **11** (2008) 16.
[79] R.J. Parro, M.C. Scardelletti, N.C. Varaljay, S. Zimmerman and C.A. Zorman // *Sol.-St. Electr.* **52** (2008) 1647.
[80] V. Gimala, J. Pezoldt and O. Ambacher // *J. Phys. D: Appl. Phys.* **40** (2007) 6386.
[81] A. Audren, A. Benyagoub, L. Thome and F. Garrido // *Nucl. Instr. Methods Phys. Res. B* **266** (2008) 2810.
[82] J. Musil, J. Vlček and P. Zeman // *Adv. Appl. Ceram.* **107** (2008) 148.
[83] S.A. Kukushkin // *Nanotechnologies in Russia* **3** (2008) 6 (English transl.).
[84] A.V. Ragulya // *Adv. Appl. Ceram.* **107** (2008) 118.
[85] M.G. Bothara. *Sintering of Nanocrystalline SiC in Plasma Pressure Compaction System. Doctor of Philosophy Dissertation in Materials Science*(Oregon State University, USA, 2007).